# ANALYSIS OF THRUSTER REQUIREMENTS AND CAPABILITIES FOR LOCAL SATELLITE CLUSTERS

G. J. Yashko†, D.E. Hastings††
Massachusetts Institute of Technology
Cambridge, Massachusetts

## Abstract

This paper examines the propulsive requirements necessary to maintain the relative positions of satellites orbiting in a local cluster. Formation of these large baseline arrays could allow high resolution imaging of terrestrial or astronomical targets using techniques similar to those used for decades in radio interferometry. A key factor in the image quality is the relative positions of the individual apertures in the sparse array. The relative positions of satellites in a cluster are altered by "tidal" accelerations which are a function of the cluster baseline and orbit altitude. These accelerations must be counteracted by continuous thrusting to maintain the relative positions of the satellites. Analysis of propulsive system requirements, limited by spacecraft power, volume, and mass constraints, indicates that specific impulses and efficiencies typical of ion engines or Hall thrusters (SPT's) are necessary to maintain large cluster baselines. In addition, required thrust to spacecraft mass ratios for reasonable size clusters are approximately 15μN/kg. Finally, the ability of a proposed linear ion microthruster to meet these requirements is examined. A variation of Brophy's method is used to show that primary electron containment lengths on the order of 10 mm are necessary to achieve those thruster characteristics. Preliminary sizing of the linear ion microthruster is given.

## Nomenclature

$A_c$ = thruster chamber area, $m^2$
b = filled aperture characteristic dimension
B = sparse aperture baseline
BDV = electric field breakdown voltage, V
$C_o$ = primary electron utilization factor, $A^{-1}$
$d_a$ = accelerator grid spacing, m
$D_{tank}$ = propellant tank diameter, m
$D_{s/c}$ = spacecraft diameter, m
e = electric charge, $1.6x10^{-19}$ C
$f_B$ = fraction of ions extracted
$f_C$ = fraction of ion current produced that goes to cathode potential surfaces, m
$F_{tot}$ = total thrust, N
$g_o$ = gravitational acceleration, 9.8 $m/s^2$
h = orbit altitude
$H_c$ = thruster chamber height, m
$I_B$ = Impulse bit, Ns
$I_{SP}$ = spacecraft mass, s
$J_B$ = ion beam current, A
$L_c$ = thruster chamber width, m
$l_e$ = primary electron containment length, m
life = mission life, s
$m_i$ = mass of propellant ion/neutral atom, kg
$m_{s/c}$ = spacecraft mass, kg
$m_p$ = total propellant mass, kg
$m_{pp}$ = power plant mass, kg
$\dot{m}_i$ = ion mass flow rate, kg/s
$\dot{m}$ = propellant mass flow rate per chamber, kg/s
$\dot{m}_{tot}$ = total thruster mass flow rate, kg/s
$N_c$ = thruster chamber width, $m^2$
$N_f$ = number of lifetime impulsive thruster firings
$n_o$ = chamber neutral atom density, $kg/m^3$
$P_{in}$ = required thruster power input, W
$P_{s/c}$ = available spacecraft power, W
$r_a$ = along-track resolution
R = reference satellite distance from Earth center
$R_s$ = slant range
S = synthetic aperture dimension
$v_o$ = neutral atom velocity, m/s
$V_{net}$ = net voltage across deceleration grid, V
$V_{tot}$ = total voltage across acceleration grid, V
$V_D$ = discharge voltage, V
$W_c$ = thruster chamber width, m
x = Displacement of cluster satellite in $\hat{x}$
y = Displacement of cluster satellite in $\hat{y}$
z = Displacement of cluster satellite in $\hat{z}$
$\alpha_{s/c}$ = spacecraft specific power, W/kg
$\alpha_{pp}$ = power plant specific power, W/kg
$\Delta V$ = velocity increment, m/s
$\varepsilon_B$ = average beam ion energy costs, eV
$\varepsilon_P^*$ = minimum plasma ion energy costs, eV
$\varphi_o$ = grid transparency to neutrals, m
$\eta$ = thruster efficiency
$\eta_u$ = propellant utilization efficiency
$\lambda$ = sensing wavelength
$\Gamma$ = thrusting per unit of spacecraft mass, N/kg
$\rho_p$ = propellant density, $kg/m^3$
$\rho_{s/c}$ = spacecraft density, $kg/m^3$
$\sigma_o$ = total inelastic collision cross section for primary electron-neutral collisions, $m^3$
$\theta$ = angular position of satellite in cluster, rad
$\theta_r$ = angular resolution, radians
$\Omega$ = satellite angular velocity

---

† Graduate Student, Member AIAA
†† Professor of Aeronautics and Astronautics, Associate Fellow, AIAA

## 1. Background

Interferometry has been used for decades to produce images of astronomical objects in radio wavelengths with resolutions rivaling that of ground-based optical systems.[1] This technique, when deployed across a cluster of satellites, may be used to produce high resolution remote sensing images of terrestrial targets from space or provide a platform above the atmosphere for space-based viewing of astronomical objects.

### 1.1 Synthetic Apertures

The diffraction limited ground resolution of typical filled apertures is given by[2]

$$r_a \approx \frac{\lambda R_s}{b}. \qquad (1)$$

Equation (1) indicates that increasing the aperture size improves the resolving power of the instrument. Aperture size is limited, however, by size and weight constraints of the launch vehicles which place the satellites in orbit. Synthetic Aperture Radar (SAR) can improve resolution at RF wavelengths from Low Earth Orbit (LEO) by utilizing the Doppler shifting of signals to "synthesize" an aperture much larger than the satellites filled aperture. Resolutions of SAR systems are given by[2]

$$r_a = \frac{b}{2} \qquad (2)$$

where b is again a characteristic dimension of the filled aperture. Although contrary to intuition, equation (2) indicates that reducing the filled aperture size improves the resolving power of the radar. At some point, however, aperture temperature, power output, and gain limitations preclude the use of smaller apertures. Table 1 lists allowable resolutions for a typical 10 m filled aperture sensing in the optical, infrared (IR), or radio frequency (RF) wavelengths at several altitudes.

Table 1. Current Achievable Resolution with 10m Aperture.

| Altitude | Optical λ=0.5μm | Infrared (IR) λ=10 μm | Radio (RF) λ=3 cm |
|---|---|---|---|
| 1,000 km | 5 cm | 1 m | 5 m (SAR) |
| 10,000 km | 50 cm | 10 m | 30 km |
| 35,768 km | 1.8 m | 18 m | 107 km |

### 1.2 Interferometry / Sparse Arrays

Another method to increase resolution is interferometry. Interferometers use separate apertures spaced some distance apart to create a sparse aperture as sketched in Figure 1.

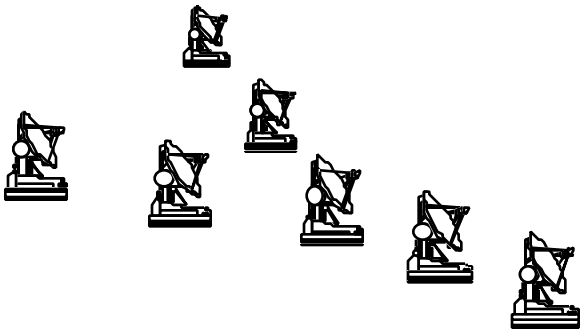

Figure 1. Ground-based Radio Interferometer

Interferometers were originally used in radio astronomy to distinguish discrete radio sources from the diffuse background. Synthesis is obtained by observing separately all the interferometer pairs that exist within a large aperture. A chessboard with only two chess pieces may be used as an analogy. All combinations of the pieces on the board must be sampled to recreate a uniform aperture. To accomplish this, the receiving elements are designed to be mobile across the so-called u-v plane. As baselines increased, the rotation of the earth was used to sweep a range of spacings with fixed antennae. Very large baselines composed of widely separated antennae soon made sampling the entire u-v plane impractical. Computer calibration techniques are now commonly used for sparse aperture synthesis[3].

The position and spacing of the elements is key to the quality of the image produced. The paths traced out by the electro-magnetic waves must be carefully controlled so that the signals may be coherently combined. This tolerance is typically λ/20. In the case of the Space Telescope's primary mirror, this margin is a few hundredths of a micron.[4] For a regularly spaced array, a positional error of a few wavelengths can cause significant sidelobes, even if the faulty positions are known exactly so that each element can be correctly phased.[5] In cases where the relative positions of the element are not known (such as with random arrays), calibrations can be carried out to improve the quality of the images providing the

relative positions do not change from one image to the next.

The achievable angular resolution is diffraction limited in accordance with the Rayleigh criteria. The size of the aperture, however, is the maximum linear distance between the individual elements. This distance is known as the baseline, B, so that[3]

$$\theta_r = \frac{\lambda}{B}. \qquad (3)$$

Table 2 lists the angular resolution versus sampled wavelengths for numerous existing interferometers along with the baseline of each system. Although aperture synthesis is well established in the radio spectrum, imaging of astronomical sources with multi-aperture interferometers is just beginning with the construction of the Infrared-Optical Telescope Array (IOTA) at the F.L. Whipple Observatory on Mount Hopkins, AZ.[6]

Table 2. Angular resolution of existing interferometers

| Interferometer | Baseline | λ | Ang. Resol. |
|---|---|---|---|
| VLBI | 8,500 km | 1cm-1m | 1e-4" to 1e-2" |
| VLA | 35 km | 1cm-5m | 0.1" to 20" |
| Westerbrook | 3.2km | 10cm-1m | 5" to 100" |
| Merlin | 135 km | 10cm-1m | 0.1" to 1" |

*Source:* Wohllenben[7], Pg 17

1.3 Local Satellite Clusters

Forming space-based sparse apertures, analogous to the ones discussed in section 1.2, could be accomplished through the use of a local satellite cluster. Satellites in a local cluster orbit in formations such as those shown in Figures 2a and 2b. Although one or more reference satellites will be in standard Keplerian (ie. inertial) orbits, maintaining the formation will require the other satellites to orbit in planes parallel to the reference orbits. These non-inertial orbits are characterized by either a focus which is not located at the Earth's center of mass (Fig 2a), or orbital velocities which do not provide the proper centripetal acceleration to offset gravity at that altitude (Fig 2b). As expected, the Earth's gravitation will act to move these satellites into Keplerian orbits. It will be shown in Section 2 that continuous low-level thrusting is required to maintain each satellites position.

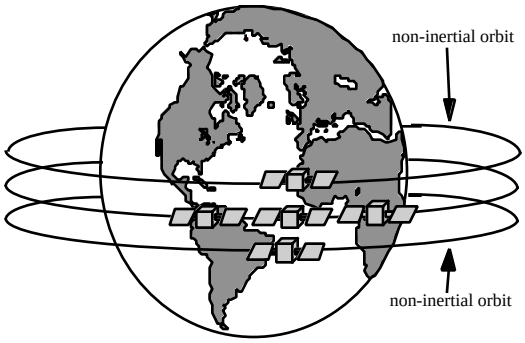


Fig. 2a. Cluster Formation Normal to Reference Orbit Plane

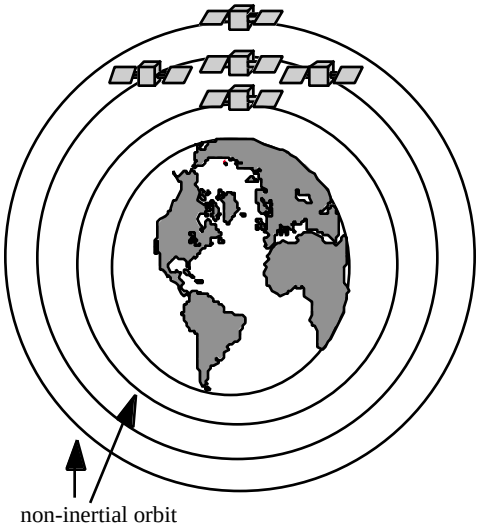


Figure 2b. Cluster Formation in Plane of Reference Orbit

By coherently adding the signals received by several satellites, the cluster would, in effect, create a sparse aperture many times the size of a real aperture. The sparse aperture's large size could vastly increase the level of resolution possible. There are several possible advantages of creating a sparse array cluster. For example:

1) Extensive earth coverage could be achieved at GEO with a resolution similar to that of current satellites in LEO.
2) By turning satellites within the cluster "on and off" it may be possible to alter the dimensions of the sparse aperture and thus zoom in on a target detected in a broad, coarse field of view.

The gravitational forces which act on the satellites in non-inertial orbits will now be examined in more detail.

## 2. Orbital Dynamics Of Satellite Clusters

### 2.1 Tidal Forces

Figure 3 shows the coordinate system for a simple two satellite cluster. Satellite 1 is in an inertial reference orbit at an distance, R, from the center of the Earth. Satellite 2's position relative to satellite 1 is $\hat{r}$.

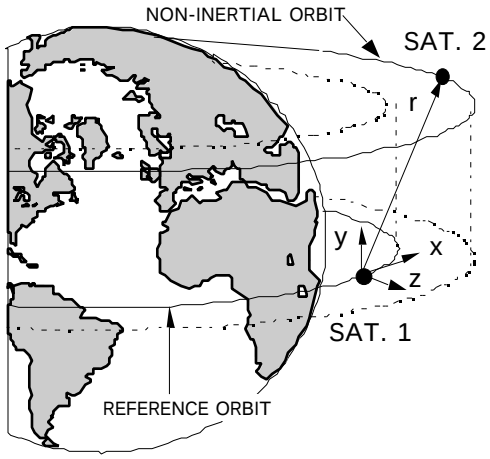


Figure 3. Satellite Cluster Coordinate System.

The motion satellite 2 with respect to 1 can be found using the linearized equations of relative motion for a circular reference orbit. These equations, known as the Clohessey-Wiltshire equations, are[8]

$$\begin{aligned} \Gamma_x &= \ddot{x} + 2\Omega\dot{z} \\ \Gamma y &= \ddot{y} + \Omega^2 y \\ \Gamma_z &= \ddot{z} + 2\Omega\dot{x} - 3\Omega^2 z \end{aligned} \qquad (4)$$

where $\Omega = \sqrt{\mu / R^3}$.

One would intuitively expect a $\Gamma_z$ term due to displacements along $\hat{y}$. It is eliminated by the linearization process in the derivation of (4), although it does appear in the full length equations.

$$\Gamma = \begin{bmatrix} \ddot{x} + 2\Omega\dot{z} \\ \ddot{y} + \Omega^2 y \\ \ddot{z} - 2\Omega\dot{x} \end{bmatrix} - \begin{bmatrix} \Omega^2 x \\ \Omega^2 y \\ \Omega^2 (R+z) \end{bmatrix} \left(1 - \frac{1}{C^{3/2}}\right) \qquad (5)$$

where $C = \left(1 + \frac{2z}{R} + \frac{x^2 + y^2 + z^2}{R^2}\right)$.

Section 3 identifies the maximum displacements from the reference orbit that are feasible due spacecraft mass, power, and volume constraints. For those size clusters, this extra $\Gamma_z$ term is negligible.

Equation (4), when multiplied by the $m_{s/c}$, describes the required on-board thrusting necessary to produce desired accelerations and velocities relative to some reference satellite in an inertial orbit. Notice that for $x = y = z = \dot{x} = \dot{y} = \dot{z} = \ddot{x} = \ddot{y} = \ddot{z} = 0$, (4) reduces to the case of a satellite in a inertial orbit where no thrusting is necessary to maintain its orbit under two-body orbit assumptions.

Even with $\dot{x} = \dot{y} = \dot{z} = \ddot{x} = \ddot{y} = \ddot{z} = 0$, y and z displacements create "tidal" forces which will tend to move the satellite into an inertial orbit as described by Janson.[9] These tidal forces need to be counteracted by thrusting in order to maintain the cluster. Tidal forces arise from displacements along $\hat{z}$ because the cluster satellite is constrained to orbit with the same velocity as the reference satellite yet at a different altitude. Thus, unlike the reference satellite, the gravitational attraction of the Earth is not exactly offset by the centripetal acceleration due to the satellite's circular motion. Displacements along $\hat{y}$ force the satellite to orbit in a plane parallel to reference satellite. In that case, only a component of the gravity vector lies in the plane of the orbit. Once again, the centripetal acceleration is not offset by Earth's gravity. A displacement along $\hat{x}$ can be considered a displacement along $\hat{z}$ occurring at a point further ahead in the reference orbit.

Tidal accelerations, which must be counteracted with thrusting, are shown in Figures 4 and 5 for displacements normal to the reference orbit plane ($\hat{y}$) and radially within the reference orbit plane ($\hat{z}$).

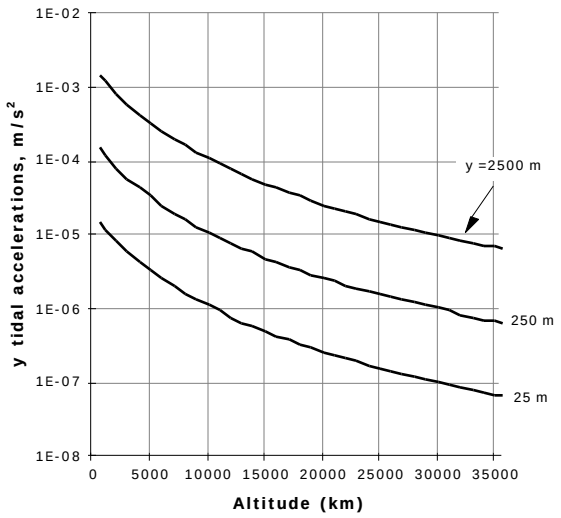


Figure. 4. Tidal accelerations along $y$ for satellite displaced a distance y.

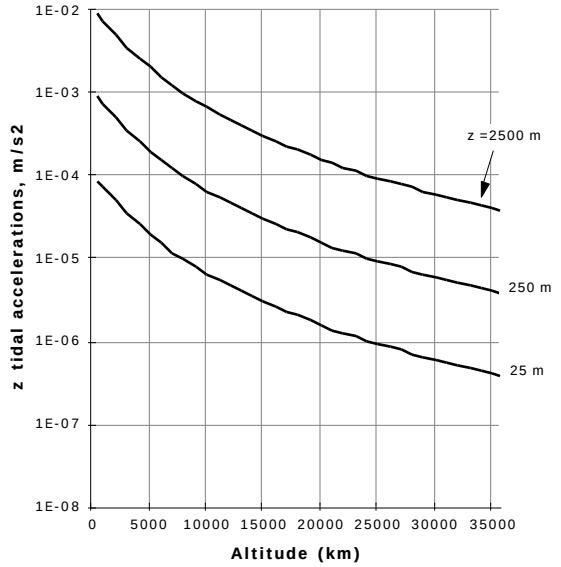


Figure. 5. Tidal accelerations along $\hat{z}$ for satellite displaced a distance z.

2.3 Impulsive vs. Continuous Thrusting

To remain within the allowable relative position tolerances discussed briefly in Section 1.3, the cluster of satellites could use either a series of impulsive thruster firings at regular intervals or apply a lower, continuous thrust.

Consider the case of a satellite displaced along $\hat{y}$ as shown in Figure 6. If no thrust were applied in the y direction, the displaced satellite would oscillate around the reference orbit completing one oscillation every orbit. In essence, it would be in an inertial orbit inclined with respect to the reference orbit. This motion relative to the reference orbit would move the satellite beyond the allowed tolerance for elements of a sparse array. Therefore, the thruster will need to fire an impulse bit which keeps the satellite within the tolerance region.

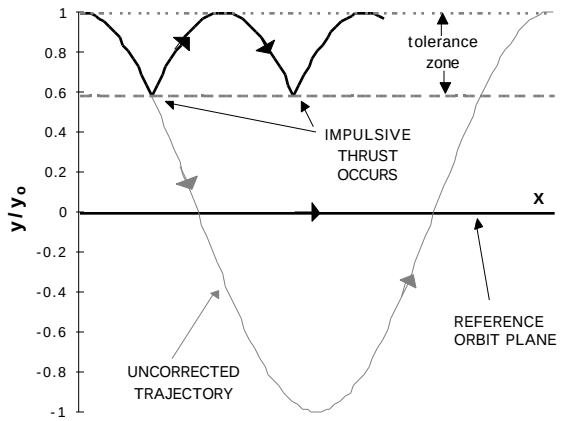


Figure 6. Impulsive Thrusting Procedure

At time t=0, halfway between impulse firings, $x = z = \dot{x} = \dot{z} = \ddot{x} = \ddot{z} = \Gamma_x = \Gamma_y = \Gamma_z = 0$. Equation (4) then reduces to

$$\ddot{y} + \Omega^2 y = 0 \tag{6}$$

This undamped linear oscillator has the solution[9]

$$y(t) = y_o \cos(\Omega t) \tag{7}$$

$$\dot{y}(t) = -y_o \Omega \sin(\Omega t) \tag{8}$$

$$\ddot{y}(t) = -y_o \Omega^2 \cos(\Omega t). \tag{9}$$

Then, from (7), the time at which the satellite would drift beyond the tolerance limit is

$$t = \frac{1}{\Omega} \cos^{-1}\left(\frac{y_o - tol}{y_o}\right) \tag{10}$$

Figure 7 shows the plot of equation (10) at several altitudes. It can be seen from the figure that, at all altitudes, as the required relative position tolerance decreases the time the satellite is able to drift before firing an impulse decreases. The largest value of tolerance/displacement will be for RF sensing sparse apertures in LEO. For an RF cluster satellite sensing

at λ=.05m, tolerances will be on the order of 2.5 mm. At 1000 km altitude and displaced 25m, this tolerance/displacement is 1e-4. Figure 7 indicates that the satellite could drift for 14 seconds. In the optical region, however, allowable drift time is approximately 0.05 seconds.

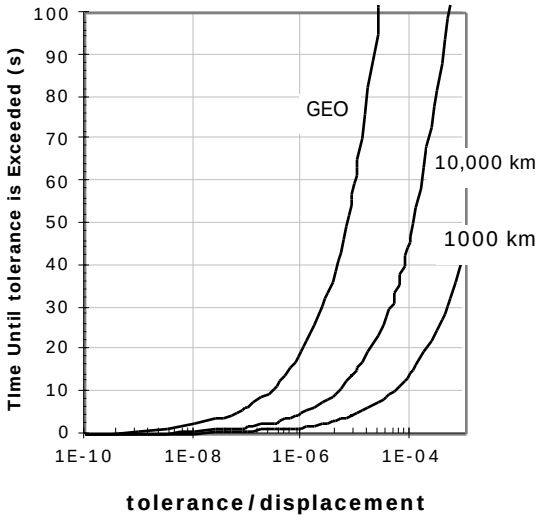


Figure. 7. Time Until Tolerance is Exceeded

Assuming that the satellite's y velocity after the impulse is exactly negative that before the impulse, and that the tidal forces and impulse thrust are constant during the time the impulse is applied, then

$$\frac{I_B}{m_{s/c}} = 2y_o\Omega\sin(\Omega t) + \left[y_o\Omega^2\cos(\Omega t)\right](\Delta t) \quad (11)$$

where t is found from (10) and Δt is the thruster firing time.

The total impulsive firings during the mission life is then

$$N_f = \frac{life}{2t + \Delta t} \quad (12)$$

Calculating the total impulsive ΔV expended over the mission life,

$$\Delta V = N_f \frac{I_B}{m_{s/c}} \quad (13)$$

Figure 8 compares the ΔV expended for continuous thrusting to that of impulse thrusting. The figure shows that for a given displacement, as the tolerance region in which the satellite can drift increases, only negligible amounts of ΔV can be saved by using impulsive thrusts. As the tolerances tighten (and the time between impulsive thrusts shortens), the ΔV expended for a impulsive thrust approaches that expended by continuous thrusting.

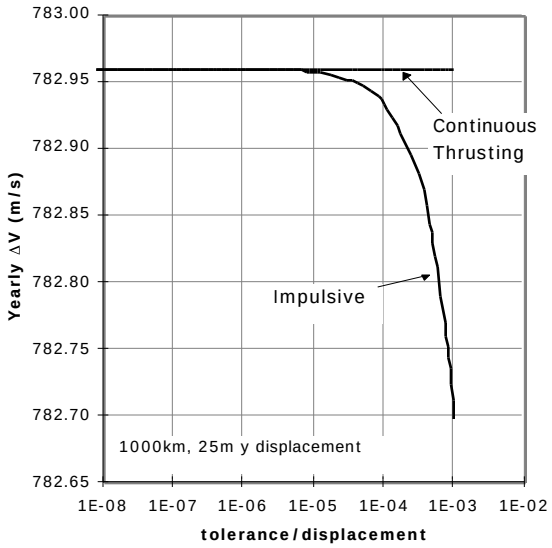


Figure 8. Propellant Savings from Impulsive Thrusting.

The previous analysis would indicated that, at the broadest relative position tolerance levels, the maximum time between required impulsive thrusts is on the order of seconds. For optical and infrared wavelengths, this time is on the order of tenths of a second. Further, at these short thrusting intervals, only minimal amounts of propellant savings result from impulsive thrusting. Therefore, continuous thrusting will be assumed for the rest of this analysis.

## 2.3 Dynamic Clusters

For the situation where satellite positions are fixed relative to each other, the total ΔV expended during the satellite's mission life is

$$\Delta\dot{V} = (\dot{\Gamma})\,life \quad (14)$$

where $\dot{\Gamma}$ is the acceleration produced continuously by an on-board propulsive system to counteract tidal forces. Equation (4) indicates that the required thrust per unit of spacecraft mass is larger for a satellite stationed at a greater distance from the reference orbit. From equation (14), for a given mission life, a satellite stationed far from the reference orbit will consume more fuel than a satellite stationed closer. It

may be desirable, therefore, to rotate the positions of the satellites during their life as a means of distributing the fuel consumption amongst all the satellites in the cluster.

Consider the case, illustrated in Figure 9, where the satellites in a cluster continually rotate in a circular pattern relative to the reference satellite. Figure 9 shows only two of the many satellites comprising the cluster. This is one of many possible methods by which satellites in a cluster change position, but it serves well as an example of a "dynamic cluster".

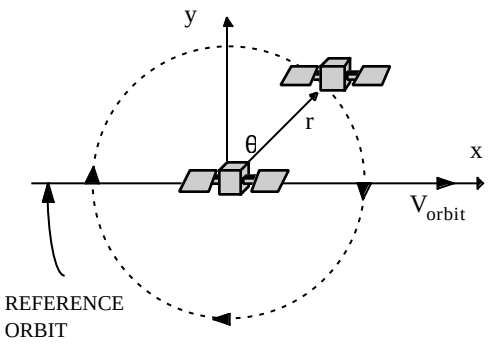


Figure 9. Dynamic Cluster Formation

For this situation,

$$\begin{aligned} x &= r\sin(\theta) \\ y &= r\cos(\theta) \\ z &= 0 \end{aligned} \qquad (15)$$

By substituting the relations from (15), equation (4) becomes

$$\begin{aligned} \Gamma_x &= -r\dot{\theta}^2\sin\theta \\ \Gamma_y &= -r\cos\theta\left(\Omega^2 + \dot{\theta}^2\right) \\ \Gamma_z &= 2r\left(\cos\theta\right)\Omega\dot{\theta} \end{aligned} \qquad (16)$$

where $\Omega = \sqrt{\mu / R^3}$.

It can be seen from (16) that the required thrust levels of a satellite in a dynamic cluster are a function of the cluster radius, r, the cluster's reference altitude, the position of the satellite, $\theta$, as well as the rate at which the satellite rotates about the reference satellite, $\dot{\theta}$. Figure 10 shows $\Delta V$ expended by all satellites in the example dynamic cluster can be as low as 54% that expended by a satellite at the far edge of a static, non-rotating cluster.

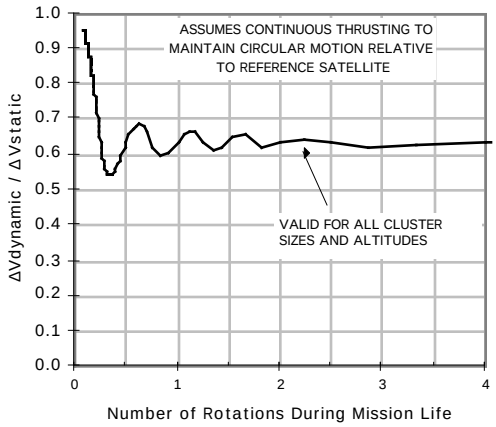


Figure 10. Reduction in Cluster Maintenance $\Delta V$

As the number of rotations about the reference satellite increases beyond about 1/3, the $\Delta V$ ratio begins to increase again because the satellite is spending more time displaced further from the reference orbit along $-\hat{y}$. At a rate of 1 rotation during the mission, the $\Delta V$ expended is about 65% that of the worst case satellite in a static cluster. The $\Delta V$ ratio levels off at this value for more than 5 rotations during the mission. Although not shown in Figure 10, as the rotation rate is increase further, the $\Delta V$ required just to maintain the circular motion around the reference satellite begins to dominate. At rate of a few hundred rotations during the mission, the $\Delta V$ ratio increases above unity indicating it no longer beneficial to rotate the cluster satellites.

It should be stated that a sparse aperture might be formed using a constellation of satellites rather than a local cluster, depending on whether the positional tolerance problem could be solved. For that situation, all satellites would orbit in inertial orbits and the sparse aperture would be formed using whatever satellites are available as they fly over the region of interest. The $\Delta V$ for maintaining that "sparse aperture" would be zero. The analysis throughout the rest of this paper, however, is focused only on the requirements of maintaining a local static cluster.

## 3. Propulsion System Requirements

Based on the acceleration levels presented in section 2, the propulsion system requirements to maintain a local satellite cluster can be calculated. The feasible range of specific impulse and efficiency, constrained spacecraft mass, volume and power considerations, is the primary characteristic to be determined.

### 3.1 Current Thruster Characteristics

Two classes of propulsion, chemical and electric, are currently used as station-keeping thrusters on-board spacecraft. Tables 3 and 4 list several types of thrusters falling within those two classes along with ranges of specific impulse and efficiency. These ranges can be displayed graphically as shown in Figure 11. This format will be used as a template for a comparison of current thruster capabilities to those required for maintaining cluster formations. It is important to point out that Figure 11 simply shows the range of Isp vs. $\eta$. If a local cluster formation requires a combination of Isp and $\eta$ which falls within the shaded box, there is no guarantee a thruster with those characteristics exists. However, if the cluster satellite needs a combination of Isp and $\eta$ which does not fall within a shaded box, then it can be said that no current thruster exists which is able to meet those requirements.

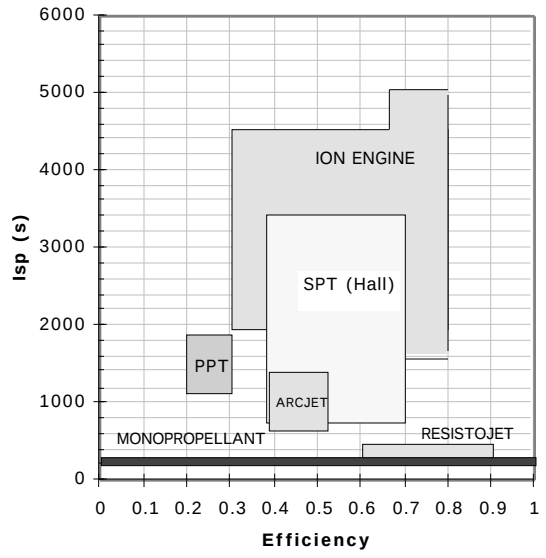


Figure 11. Current Thruster Capabilities

### 3.2 Methodology

In determining the feasible range of thruster Isp and $\eta$ necessary to maintain a local satellite cluster, the following assumptions were made:

- The satellites operate as a static cluster maintaining a fixed displacement normal to the reference orbit.
- Isp and $\eta$ are the same for all thrusters used in cluster maintenance and station-keeping
- Thrust levels of each thruster are constant during the life of the mission.
- Any cluster maintenance and station-keeping maneuvers are performed continuously.
- The spacecraft and propellant tanks are spherical.
- Spacecraft total mass is constant throughout the life of the mission.
- An additional 50m/s of propellant per year is allocated for traditional stationkeeping requirements.

A spacecraft displaced a given distance from the reference orbit using a thruster operating at a given $\eta$ and $I_{sp}$ must satisfy the following three design constraints.

$$\cdot \quad \frac{D_{tank}}{D_{s/c}} < \left(\frac{D_{tank}}{D_{s/c}}\right)_{\max}$$

$$\cdot \quad \frac{m_p + m_{pp}}{m_{s/c}} < \left(\frac{m_p + m_{pp}}{m_{s/c}}\right)_{\max} \qquad (17)$$

$$\cdot \quad \frac{P_{in}}{P_{s/c}} < \left(\frac{P_{in}}{P_{s/c}}\right)_{\max}$$

The values for the maximum ratios allow margin for the satellite to accomplish tasks other than simply operating the thrusters. Specifically, the three statements gauge whether or not there is, once station-keeping requirements have been met, sufficient volume, mass, and power available on board the satellite to perform mission operations such as payload, communications, etc. If the answer to one or more of these criteria is no, then it is concluded that a satellite of mass, $m_{s/c}$, and propellant mass fraction, $m_p/m_{s/c}$ is *unable* to adequately maintain its position, $\dot{r}$, from the reference orbit at an altitude, h, for a mission time, life, using a thrusters with specific impulse, Isp and efficiency $\eta$.

Table 3. Current Chemical Thruster Characteristics

| SYSTEM | PROPELLANT | Isp (s) | THRUST (N) |
|---|---|---|---|
| **COLD GAS*** | $N_2$, $NH_3$, Freon, Helium | 50-75 | 0.05-200 |
| **SOLID MOTOR*** | ‡ | 280-300 | 50 - $5x10^6$ |
| **LIQUID** | | | |
| MONOPROPELLANT* | $H_2O_2$, $N_2H_4$ | 150-225 | 0.05 - 0.5 |
| MONOPROPELLANT** | $N_2H_4$ | 200-230 | 0.03 - 100 |
| BIPROPELLANT* | $O_2$ and RP-1 | 350 | 5 - $5x10^6$ |
| | $O_2$ and $H_2$ | 450 | 5 - $5x10^6$ |
| | $N_2O_2$ and MMH ($N_2H_4$, UDMH) | 300-340 | 5 - $5x10^6$ |
| | $F_2$ and $N_2H_4$ | 425 | 5 - $5x10^6$ |
| | $OF_2$ and $B_2H_6$ | 430 | 5 - $5x10^6$ |
| | $CIF_5$, $N_2H_4$ | 350 | 5 - $5x10^6$ |
| WATER ELECTROLYSIS* | $H_2O$ ‡ $H_2 + O_2$ | 340-380 | 50 - 500 |
| **HYBRID*** | $O_2$ and rubber | 255 | 250 - $3.5x10^6$ |

*SOURCES:*
‡ Organic polymers + ammonium percholorate + powdered aluminium
* Larson & Wertz[2]
** Sutton[10]

Table 4. Current Electric Propulsion Characteristics

| SYSTEM | PROPELLANT | Isp (s) | EFFICIENCY | THRUST (N) |
|---|---|---|---|---|
| **ELECTROTHERMAL** | | | | |
| RESISTOJET* | $N_2$, $NH_3$, $N_2H_4$, $H_2$ | 150 - 700 | | $5x10^{-6}$ - 0.5 |
| RESISTOJET** | $NH_3$, $N_2H_4$, $H_2$ | 200 - 300 | 65 - 90 | 0.002 - 0.1 |
| ARCJET* | $NH_3$, $N_2H_4$, $H_2$ | 450 - 1500 | | 0.5 - 5 |
| ARCJET** | $NH_3$, $N_2H_4$, $H_2$, $N_2$ | | 40 - 50 | 0.002 - 0.7 |
| **ELECTROSTATIC** | | | | |
| ION ENGINES* | Hg/A/Xe/Cs | 2000 - 6000 | | $5x10^{-6}$ - 0.5 |
| ION CONTACT** | Cs, Hg | 1500 - 5000 | 60 - 80 | $1x10^{-6}$ - 0.1 |
| ION BOMBARDMENT*** | Xe, Hg, Ar,Kr | 1500 - 5000 | 60 - 80 | $1x10^{-5}$ - 0.2 |
| COLLOID* | Glycerine | 1200 | | $5x10^{-6}$ - 0.5 |
| **ELECTROMAGNETIC** | | | | |
| SPT (HALL)*** | Xe | 800 - 3000 | 37 - 71 | 0.015 - 0.26 |
| MPD* | Argon | 2000 | | 25 - 200 |
| MPD ARCJET** | | | 30 - 50 | $1x10^{-6}$ - 2 |
| HALL EFFECT MPD** | Cs, Bi, Ar, $N_2$, Xe, $H_2$ | | 30 - 50 | $1x10^{-5}$ - 2 |
| PPT* | Teflon | 1500 | | $5x10^{-6}$ - 0.005 |
| SOLID PULSED PLASMA** | Teflon | 1000 - 2000 | 20 - 30 | $5x10^{-5}$ - 0.01 |
| PULSED INDUCTIVE* | $N_2H_4$ | 2500 | | 2-200 |

*SOURCES:*
* Larson & Wertz[2]
** Sutton[10]
*** G. Malyshev et. al.[11]

The values for the three constraints listed above can be found as follows:

1. For a given cluster size and altitude, the accelerations along $\hat{y}$ can be found by evaluating equation (4).

2. The corresponding thrust to counteract those accelerations is given by

$$\vec{F}_{tot} = m_{s/c}\vec{\Gamma}$$

3. Knowing the acceleration and assuming continuous thrusting, the total $\Delta V$ required is

$$\Delta V_{tot} = (\Gamma_x + \Gamma_y + \Gamma_z)(life)$$

4. The total propellant used during the life of the mission is simply

$$m_p = \left(1 - e^{-\Delta V / I_{sp} g_o}\right) m_{s/c}$$

5. The diameter of the spacecraft is

$$D_{s/c} = \left(\frac{6}{\pi} \frac{m_{s/c}}{\rho_{s/c}}\right)^{\frac{1}{3}}$$

6. Using $m_p$, the diameter of the propellant tank is

$$D_{tank} = \left(\frac{6}{\pi} \frac{m_p}{\rho_p}\right)^{\frac{1}{3}}$$

7. The total power available to the spacecraft is

$$P_{s/c} = m_{s/c}\alpha_{s/c}$$

8. For electric propulsion, a power plant is required on-board the satellite to provide power to the thruster. Therefore, the maximum required input power to the thrusters, using the current value of Isp being evaluated and thrust levels from step 2 is

$$P_{in} = \frac{I_{sp} g (F_{max})}{2\eta} \qquad (18)$$

9. The mass of the power plant can be found using input power calculated in step 8 along with the specific power of the power plant

$$m_{pp} = \frac{P_{in}}{\alpha_{pp}}$$

Table 5 lists the maximum values chosen for these constraints as well as other input parameters.

Table 5. Baseline parameters

| | |
|---|---|
| $\alpha_{pp}$ | 10 W/kg |
| $\alpha_{s/c}$ | 2 W/kg |
| $\rho_p$ | 500 kg/m$^3$ |
| $\rho_{s/c}$ | 79 kg/m$^3$ |
| life | 5 yrs |
| $m_p/m_{s/c}$ | .1 |
| $m_{s/c}$ | 100 kg |
| $(m_p/m_{s/c})_{max}$ | 0.1 |
| $(P_{in}/P_{s/c})_{max}$ | 0.20 |
| $(D_{tank}/D_{s/c})_{max}$ | 0.33 |
| $[(M_p+M_{pp})/M_{s/c}]_{max}$ | 0.30 |

### 3.3 Analysis of Cluster Missions

The methodology developed in section 3.2 can now be used to determine the range of thruster specific impulse and efficiency which can maintain the relative positions of a satellite in a cluster without exceeding the satellite design ratios.

Figures 12 through 14 illustrate the feasible regions of thruster specific impulse vs. efficiency for clusters orbiting at various altitudes. At specific impulses below the feasible regions, the required propellant to maintain the cluster during the five year mission life exceeds the assumed 10% maximum initial propellant mass fraction. In actuality, the thruster must operate at an $I_{sp}$ above this lower limit since propellant utilization, $\eta_u$=1, is assumed in this initial analysis. Combinations of specific impulse and efficiency above and to the left of the feasible regions result in thruster power requirements greater than the allowable 20% of spacecraft power. Because the thruster power is determined by equation (18), an increase in thruster efficiency allows for higher specific impulses without exceeding the power limitations.

As shown in Figure 12, a satellite in a cluster orbiting at 1000 km altitude with a 25 m baseline requires thrusters operating at a minimum specific impulse and efficiency of 2000s and 40% respectively. SPT's and ion engine technology can currently achieve these ranges. If the baseline is increase to 35 m, thruster requirements increase to 2700s specific impulse and 80% efficiency.

Similar effects can be seen for clusters orbiting at 10,000 km (Fig. 13) and at GEO (Fig. 14). At 10,000 km, cluster baselines in the hundreds of meters can be achieved using SPT or ion engine technologies. These baselines increase to 4000-6000 m for clusters stationed at GEO. An important point to notice is that at no altitude can chemical propulsion maintain cluster formations for the 5 year lifetime.

The achievable resolutions from the sparse aperture baselines shown in Figures 12 through 14 are listed in Tables 5 and 6.

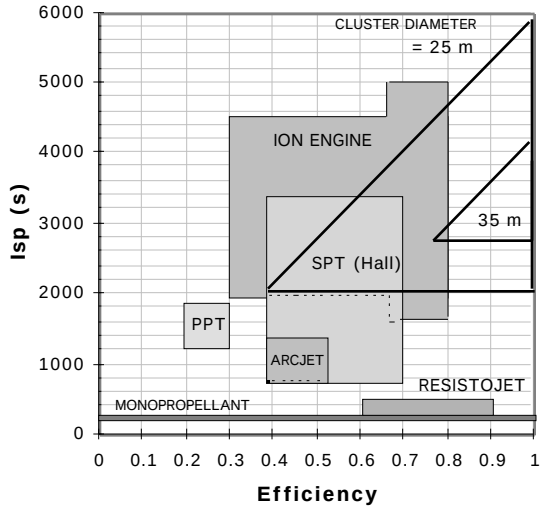


Figure 12. Feasible Isp vs. η at 1,000 km

Moving a cluster to higher orbits dramatically increases the allowable baselines for sparse apertures. However, due to the increased range to target from GEO, ground resolutions increase by only about a factor of 5 (see Table 5).

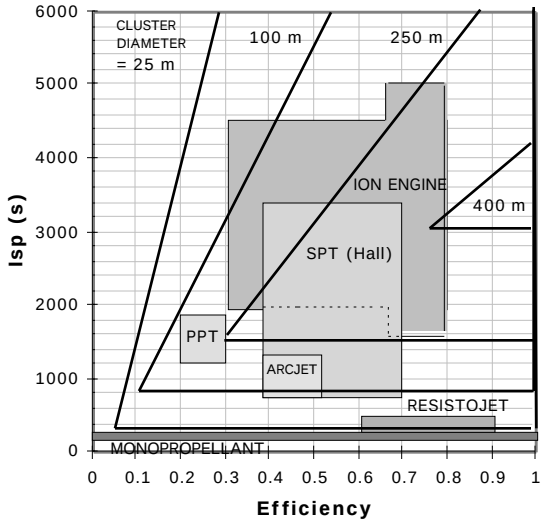


Figure 13. Feasible Isp vs. η at 10,000 km

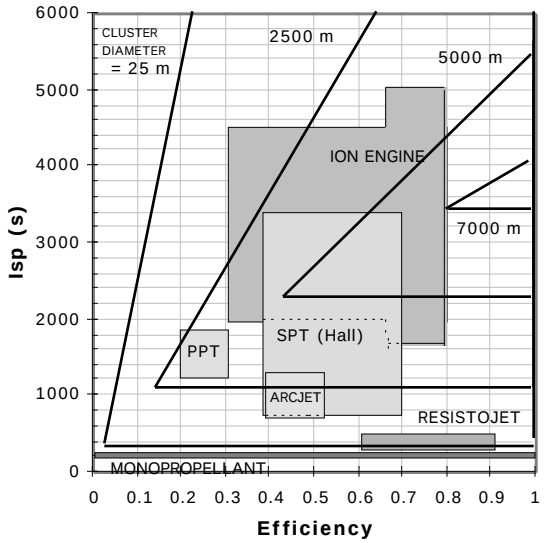


Figure 14. Feasible Isp vs. η at GEO

Table 5. Feasible Sparse Aperture Ground Resolution

| ALTITUDE | CLUSTER BASELINE | VISIBLE (.5μm) | IR (10μm) | RF (5cm) |
|---|---|---|---|---|
| 1000 km | 25 m | 20 mm | 40 cm | 2 km |
| | 35 m | 14 mm | 29 cm | 1.5 km |
| 10,000 km | 25 m | 200 mm | 400 cm | 20 km |
| | 100 m | 50 mm | 100 cm | 5 km |
| | 200 m | 25 mm | 50 cm | 2.5 km |
| | 400 m | 13 mm | 25 cm | 1.3 km |
| 35768 km | 25 m | 710 mm | 15 m | 72 km |
| | 2000 m | 9 mm | 18 cm | 900 m |
| | 5000 m | 4 mm | 7 cm | 350 m |
| | 7000 m | 3 mm | 5 cm | 250 m |

For mission where angular resolution is the main concern (such as for imaging of astronomical objects), Table 6 shows that angular resolution can be increased by a factor of order 1000 if the cluster is positioned in GEO rather than LEO. These values can be compared with the angular resolutions given for terrestrial interferometers in Table 2.

Table 6. Achievable Sparse Aperture Angular Resolutions

| ALTITUDE | CLUSTER BASELINE | VISIBLE (.5μm) | IR (10μm) | RF (5cm) |
|---|---|---|---|---|
| 1000 km | 25 m | $4x10^{-3}$ ″ | $82x10^{-3}$ ″ | 412″ |
| | 35 m | $3x10^{-3}$ ″ | $59x10^{-3}$ ″ | 294″ |
| 10,000 km | 25 m | $4x10^{-3}$ ″ | $82x10^{-3}$ ″ | 412″ |
| | 100 m | $1x10^{-3}$ ″ | $20x10^{-3}$ ″ | 103″ |
| | 250 m | $412x10^{-6}$ ″ | $8x10^{-3}$ ″ | 40″ |
| | 400 m | $258x10^{-6}$ ″ | $5x10^{-3}$ ″ | 25″ |
| 35768 km | 25 m | $4x10^{-3}$ ″ | $82x10^{-3}$ ″ | 412″ |
| | 2000 m | $51x10^{-6}$ ″ | $1x10^{-3}$ ″ | 5″ |
| | 5000 m | $20x10^{-6}$ ″ | $415x10^{-6}$ ″ | 2″ |
| | 7000 m | $15x10^{-6}$ ″ | $294x10^{-6}$ ″ | 1.5 ″ |

Figure 15 shows the thrust levels per unit of spacecraft mass required by a satellite displaced from the reference orbit by 15m, 150m, and 2750m (30 m, 300m, 5500m cluster baselines respectively). These values were found using the full length equation (5). Combinations of cluster baselines and altitudes which can be achieved with moderate propulsive requirements (Figs. 12 through 14) are all seen from Figure 15 to require thrust levels on the order of 15μN per kg of spacecraft mass along $\hat{y}$. Thrust/mass along $\hat{z}$ is approximately 5 orders of magnitude smaller, justifying the use of the linearized equation (4). In addition, thrust levels along $\hat{x}$ equal zero.

This is also apparent in Figure 16 which shows the required ΔV for a five year mission. The ΔV expended in $\hat{z}$ is negligible compared to that expended in $\hat{y}$.

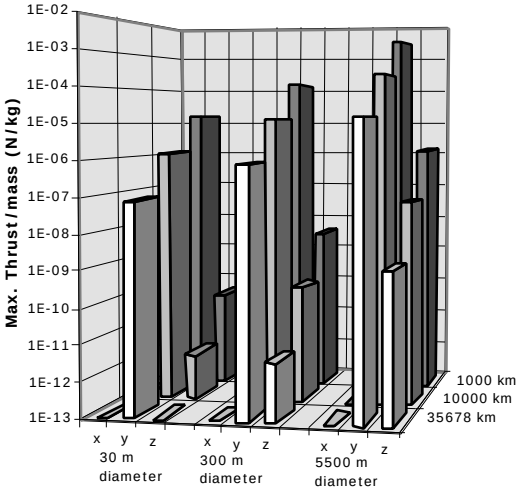


Figure 15. Thrust/mass Levels

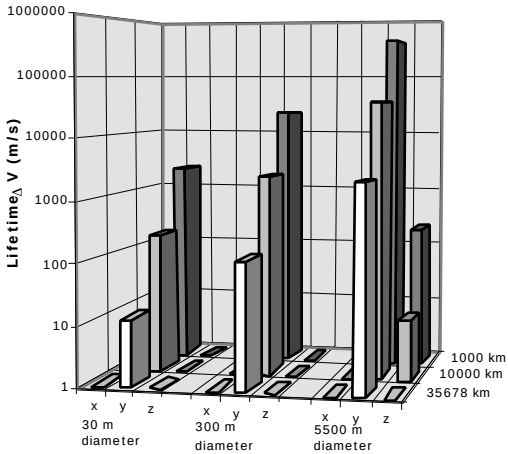


Figure 16. Required ΔV

## 4. Design of Candidate Thruster

Although any type of thruster can support a small cluster formation for a short time period, the analysis of Section 3 demonstrates that to maintain reasonable cluster baselines at a given altitude for a five year mission requires continuous thrusting by a propulsive system operating at approximately 2200-3200s specific impulse, 50-70% efficiency, and at thrust-to-spacecraft mass ratios on the order of 15μN/kg. Thus, a 100 kg satellite would require approximately 1.5 mN of thrust to maintain its position at the far edge of the cluster. As an extension of this analysis, the ability of a proposed Linear Ion Microthruster to meet these requirements is evaluated.

4.1 Linear Ion Microthruster

The linear ion microthruster, shown in Figure 17, is a concept for a micro-machined ion propulsion system proposed by members of the Jet Propulsion Laboratory.[12] The thruster consists of several linear discharge chambers situated parallel to each other. Each discharge chamber has dimensions of approximately 100µm x 300µm x 10 cm. The walls separating the discharge chambers are built up from alternating layers of conducting and insulating materials.

Two methods to produce ions are proposed by JPL. The first is the use of radio frequency discharge. Contained within the walls is the ion accelerator system which includes the RF "ionizing coil", the ion accelerator grid, and the ion decelerator grid. The second concept is based on a direct-current (DC) discharge utilizing doped diamond films as cold cathode emitters.

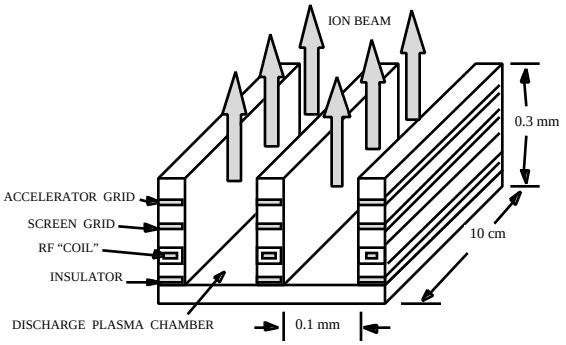


Figure 17. Linear Ion Microthruster

The scale and geometry of the linear ion microthruster is very similar to that of solar array cells. These solar cells, when operating at high negative voltages in the ionospheric plasma, have experienced arcing in the regions near the cell interconnectors. This mechanism may be exploited as an alternative method to produce ionization within the linear ion microthruster discharge chamber.

4.2 Possible Alternate Ionization Mechanism

Figures 18 and 19 illustrate the analogy between the solar array arcing mechanism and its use as the ionization mechanism of the microthruster. According to the theory developed Cho and Hastings[13], the arcing in a solar array occurs as follows:

1) Ions from ambient plasma charge the top surface of the solar array dielectric resulting in a strong electric field at the triple junction.
2) The electric field causes electrons to be emitted from the conductor provided there existed an enhanced field electron emission site on the conductor surface. Some electrons hit the dielectric side surface releasing secondary electrons on impact thereby further enhancing the electric field.
3) The intense electron current incident to the dielectric causes a dense, localized neutral cloud to form over the dielectric side surface due to electron stimulated desorption. The positive space charge resulting from the electron-collisional ionization in the neutral cloud further enhances the electric field at the conductor surface, leading to a discharge from the neutral cloud. Results show the arc emits a plasma cloud which also discharges the surfaces in the neighborhood of the arc.
4. The charging of the dielectric surface then repeats.

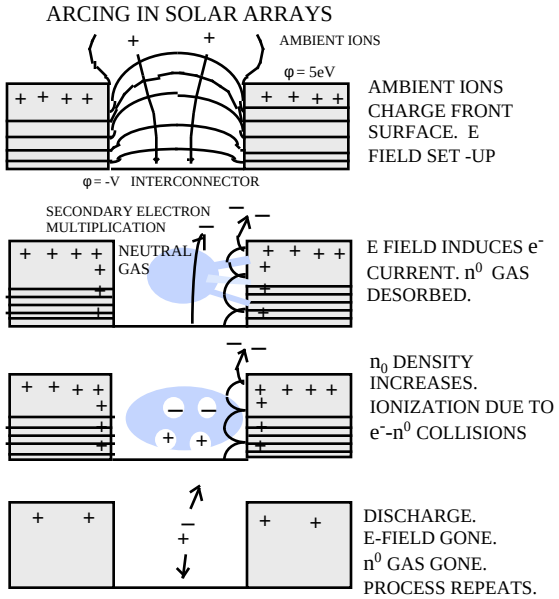


Figure 18. Solar Array Arcing Mechanism

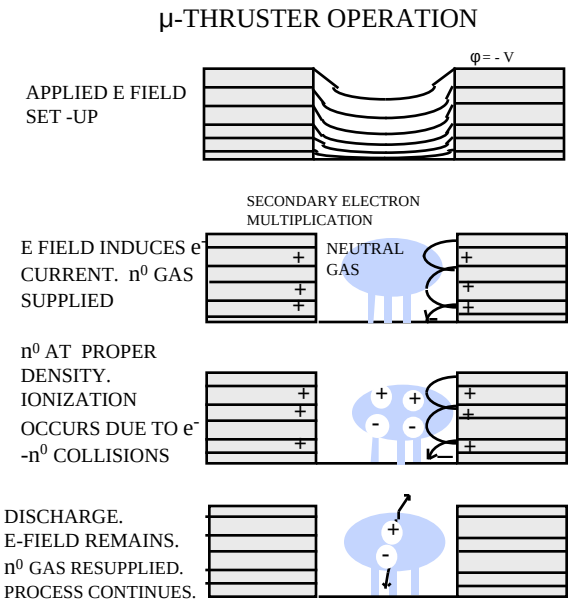


Figure 19. Alternate μThruster Ionization Mechanism

A possible advantage of this mechanism is the "hopping" of the electron up dielectric sidewall as it moves within the electric field. This trajectory acts to keep the electron within the chamber longer, making it a more effective ionizer.

A Particle in Cell (PIC) code[13] has been develop at MIT based on the solar cell arcing theory and has been compared against the Solar Array Module Plasma Interactions Experiment (SAMPIE) which flew on the Space Shuttle Columbia in March, 1994.[14] Figure 20 is a plot of arcing rate vs. bias voltage from the flight experiment and PIC code.

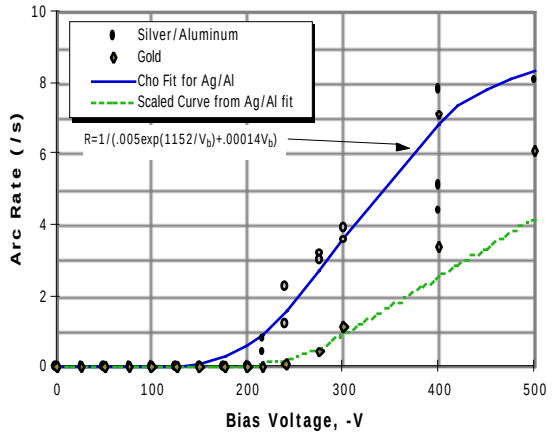


Figure 20. Solar Array arcing rates (flight data and PIC code simulation)

Other than the fact that the PIC code predicted the flight experiment arcing rate very well, one should notice that a "turn on" voltage for the arcing is present at about 200 V. This will become a factor in the section 4.2 when we discuss the Brophy Model analysis of the linear ion microthruster.

## 4.2 Brophy Model Analysis

The performance of an ion thruster is gauged by the power required to produce, but not accelerate, an ion which eventually becomes part of the beam. The average energy cost to produce a single beam ion, $\varepsilon_B$, is a key parameter in the measure of the thrusters performance. To produce a more efficient thruster it is necessary to reduce the value of $\varepsilon_B$ while maintaining a high propellant utilization. The model developed by Brophy and Wilbur[15] for predicting $\varepsilon_B$ in ring and line cusp ion thrusters can be modified to facilitate the design of the linear ion microthruster.

The average beam ion energy cost is given as

$$\varepsilon_B = \frac{\varepsilon_P^*}{f_B\left\{1-\exp\left[-C_o\dot{m}\left(1-\eta_u\right)\right]\right\}} + \frac{f_C}{f_B}V_D \qquad (19)$$

where the $C_o = 4\sigma_o l_e/m_i v_o A_g \phi_o$ and $\dot{m}$ is the mass flow rate per chamber in kg/s.

Equation (19) indicates that it is desirable to maximize the value of the primary electron containment length, $l_e$ in order to reduce the power needed to create beam ions. In other words, the longer an average primary electron remains in the chamber before being lost to the anode, the more effective an ionizer it is and, consequently, the more efficient the thruster will be. Ring and line cusped ion engines as well as SPT's increase $l_e$ by employing magnets which cause the electrons to spiral around magnetic field lines.

In more general terms, $\varepsilon_B$ can be thought of as

$$\varepsilon_B = (\text{Total Power} - \text{Useful Power})/J_B \qquad (20)$$

where useful power=$J_B(V_D+V_{net})$ and total power=$P_{in}$.

Substituting $P_{in}$ from equation (20), the efficiency, $\eta$, of the thruster can then be related as:

$$\eta = \frac{P_{beam}}{P_{in}}$$

$$\eta = \frac{V_{net}}{V_D + V_{net} + \varepsilon_B}$$

$$\eta = \left[1 + \frac{(V_D + \varepsilon_B)2e}{(g_o I_{sp})^2 m_i}\right] \qquad (21)$$

Figure 21 shows efficiencies plotted versus specific impulse as calculate using equation (21) for several values of $\varepsilon_B$. For a given thruster configuration (constant $V_D$, $\varepsilon_P^*$, $f_C$, $f_B$) , equation (19) says that $\varepsilon_B$ is a function of propellant utilization, $\eta_u$, and mass flow rate, $\dot{m}$. Intuitively, the curves in Figure 21 can be interpreted as follows:

Along a constant $\varepsilon_B$ line,

If $I_{sp} \uparrow$ , then $V_{net} \uparrow$.

For constant thrust, if $V_{net} \uparrow$, then $V_{tot} \downarrow$.

If $V_{tot} \downarrow$, then $\dot{m}_i \downarrow$.

For constant $\eta_u$, if $\dot{m}_i \downarrow$ then $\dot{m} \downarrow$.

If $\dot{m} \downarrow$ then $n_o \downarrow$ since

$$n_o = \frac{4\dot{m}(1-\eta_u)}{m_i v_n A_c \phi_o} \qquad (22)$$

With a lower $n_o$, $C_o$ (i.e. $l_e$) must $\uparrow$ to maintain constant $\varepsilon_B$.

Alternatively, for constant $\dot{m}$ ,if $\dot{m}_i \downarrow$ then $\eta_u \downarrow$.

If $\eta_u \downarrow$, then $n_o \uparrow$ by (22)

$C_o$ (i.e. $l_e$) must $\downarrow$ to maintain constant $\varepsilon_B$.

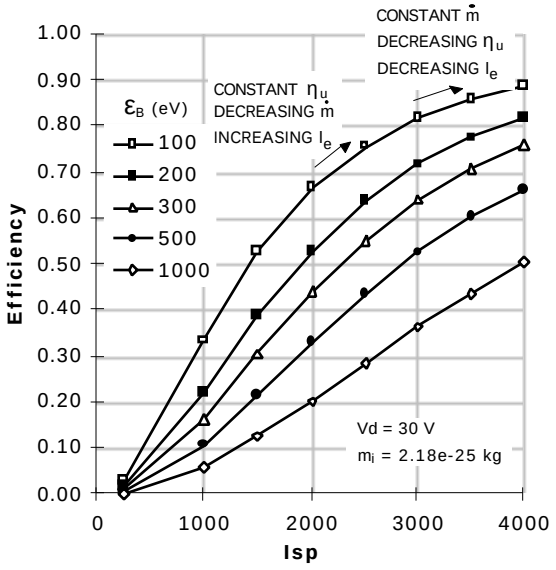


FIGURE 21. $\eta$ vs. Isp at Several $\varepsilon_B$

Therefore, if one desires a thruster to operate at a certain Isp and $\eta$, Figure 21 specifies what the average ion energy cost per beam ion needs to be subject to some combination of $\dot{m}$, $\eta_u$, and $l_e$ to be determined in section 4.3.

4.3 Minimum Required Confinement Length, le

The stated goal to this point has been to maximize the value of the primary electron confinement length, $l_e$, for the purpose of increasing the efficiency of the thruster. We now reverse this analysis and ask what is the minimum value of $l_e$ for which a thruster could operate at a given $I_{sp}$, $\eta$, and total thrust, $F_{tot}$?

Solving equation (19) for $l_e$ yields

$$l_e = \frac{-\ln\left[1 - \frac{\varepsilon_p^*}{f_B\varepsilon_B - f_C V_D}\right] m_i v_n A_c N_c \varphi_o}{\dot{m}_{tot}(1-\eta_u)4\sigma_o} \qquad (23)$$

where $\dot{m}_{tot}$ is the total propellant mass flow rate for all chambers in kg/s.

Assuming 1-D space charge limited ion mass flow rate, then

$$\frac{V_{tot}^{3/2}}{d_a^2} A_c N_c = \frac{9}{4}\frac{\dot{m}_{i\,tot}}{\varepsilon_o}\left(\frac{e}{2m_i}\right)^{0.5} \qquad (24)$$

where $\dot{m}_{i\,tot}$ is in kg/s.

For a given thrust level

$$\dot{m}_{i\,tot} = \frac{F_{tot}}{I_{sp} g_o} \qquad (25)$$

Therefore, the LHS of (24) is a constant. Thruster design iterations which change $V_{tot}$, $d_a$, $A_c$, or $N_c$ must do so in accordance with (24) in order to maintain a constant $F_{tot}$.

Using the fact that $\dot{m}_{i\,tot} = \dot{m}_{tot}\eta_u$ and substituting (24) and (25) into (23) gives

$$l_e = \frac{-\ln\left[1 - \frac{\varepsilon_p^*}{f_B\varepsilon_B - f_C V_D}\right] m_i v_n \varphi_o I_{sp} g_o}{\frac{F_{tot}}{A_c N_c}\frac{(1-\eta_u)}{\eta_u} 4\sigma_o} \qquad (26)$$

Equation (26) says that for a linear ion microthruster operating at a given $\varepsilon_B$ (i.e. Isp and $\eta$ from Fig. 21), the required primary electron containment length can be minimized by decreasing $\eta_u$ or decreasing the quantity $A_cN_c$. By equation (24) decreasing $A_cN_c$ is equivilent to increasing $V_{tot}^{3/2} / d_a^2$.

The amount by which $\eta_u$ and $A_cN_c$ can be reduced are limited by several constraints..

1. The amount of propellant required can not exceed the initial propellant mass fraction of 10%, i.e.,

$$\frac{\dot{m}_{ion}}{\eta_u}\, life < \left(\frac{m_p}{m_{s/c}}\right) m_{s/c} \qquad (27)$$

2. At very low thrust levels, it would be possible to reduce $l_e$ by operating the linear ion microthruster at very low values of $\eta_u$ and still remain below 10% propellant mass fraction. Although it could accomplish the mission, such a thruster would require a lot of propellant for little thrust provided. Therefore, a minimum operating $\eta_u$ will be assumed. Figure 22 shows the additional reduction in $l_e$ possible by continuing to reduce $\eta_u$. An "elbow" in the curve appears around 0.6. For $\dot{m}$ , the elbow occurs at $\eta_u$ =0.3. Splitting the difference the minimum operating is

$$\eta_u > 0.45. \qquad (28)$$

3. The electric field across the accelerator "grid" can not exceed the breakdown limit, i.e,

$$\frac{V_{tot}}{d_a} < BDL \approx 10^6 \frac{V}{m} \qquad (29)$$

The exponents in the ratio $V_{tot}^{3/2} / d_a^2$ indicate that, to minimize $l_e$, $d_a$ should be made as small as possible (within manufacturability limits) even though equation (29) will force $V_{tot}$ to be reduced.

4. The voltage across the accelerator grids must be greater than the net voltage across the deceleration grid to prevent backstreaming of electrons into the chamber A high value of $V_{net}/V_{tot}$ is desired so that $d_a$ can be reduced. Therefore,

$$Vtot = Vnet / 0.8$$

5. The minimum average beam ion energy cost must be greater than 200 eV. This requirement stems from results of the SAMPIE flight experiment data and Cho PIC codes simulation (Figure 20) that indicate a minimum bias voltage of 200 V is needed to initiate the arcing mechanism.

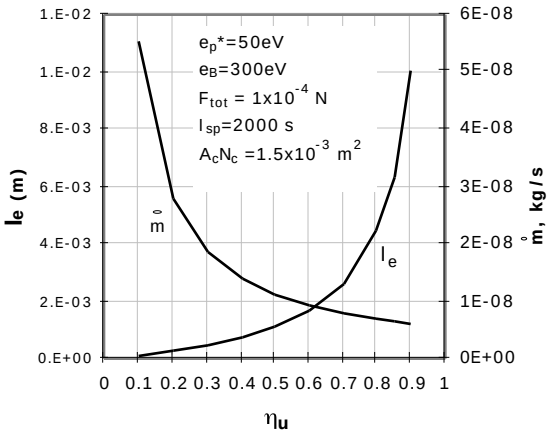


Figure 22. Mass flow rate and containment length vs. $\eta_u$

Table 7 list addition assumptions used in determination of the minimum allowable primary electron confinement length.

Table 7. Brophy Model Assumptions

| | |
|---|---|
| $\varepsilon_P^*$ | 50 eV |
| $V_D$ | 30 V |
| $f_B$ | 0.95 |
| $f_C$ | 0.05 |
| $m_i$ | $2.18\times10^{-25}$ kg |
| $T_n$ | 450 K |
| $\sigma_o$ | $2.18\times10^{-20}$ m$^2$ |
| $\varphi_o$ | 1 |

Figures 23, 24, and 25 show the minimum required primary electron containment length, $l_e$, versus efficiency at several values of specific impulse for thrust to mass ratios (ie. required accelerations) equal to, $0.1\times10^{-6}$, $1\times10^{-6}$, and $15\times10^{-6}$ respectively.

- For a given thrust to spacecraft mass ratio and $\eta$, an increase in $I_{sp}$ reduces required $l_e$ because, from Figure 21, the average beam ion energy costs $\varepsilon_B$ is allowed to increase.
- For a given thrust to spacecraft mass ratio and $I_{sp}$, an increase in $\eta$ increases required $l_e$ because, again from Figure 21, $\varepsilon_B$ is decreasing. For this situation, an upper limit on allowable $\eta$ exists

due to the constraint that $\varepsilon_B$ is greater than 200 eV. A lower limit on allowable $\eta$ exists due to spacecraft power limitations of equation (17).

- For a given $I_{sp}$ and $\eta$, as the thrust to spacecraft mass ratio increases, $l_e$ increases because a larger fraction of the propellant must be utilized to produce thrust (i.e. $\eta_u \uparrow$). At any thrust to spacecraft mass ratio less than $0.1 \times 10^{-6}$ (Fig. 23), no further reduction in $l_e$ is possible without violating the minimum operating $\eta_u$ given by equation (28). Also as the thrust to mass ratio increases, the minimum $I_{sp}$ which the thruster operates increases due to initial propellant mass fraction constraints.
- Operating at $\eta_u$ lower than that listed with $I_{sp}$ along side each curve in Figures 23 through 25 would violate the initial propellant mass fraction constraints. Operating at higher $\eta_u$ would result in a larger required value of $l_e$.

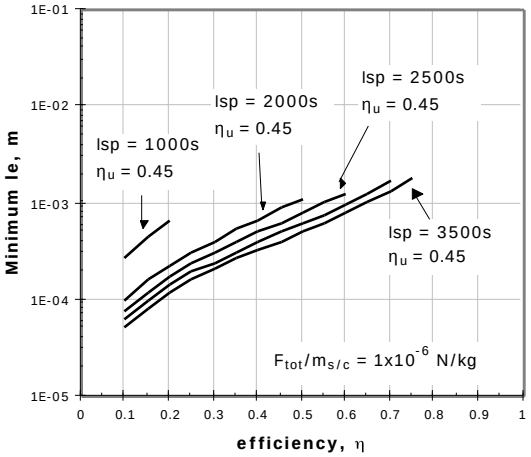


Figure 23. Minimum $l_e$ for $F_{tot}/m_{s/c} = 1 \times 10^{-6}$ N/kg

It was concluded in Section 3.3 that a reasonable cluster baseline would need thrust to spacecraft mass ratios of approximately 15μN/kg. A thruster operating at this acceleration level and at $I_{sp}$=2500 would, from Fig. 25, need a primary electron confinement length, $l_e$, equal to a few centimeters. Increasing the specific impulse at which the thruster operates to 3000 s reduces $l_e$ to a few millimeters which is more on the scale of the linear ion microthruster. Additionally, the $\eta_u$=0.8 corresponding to $I_{sp}$=3000 s is more realistic.

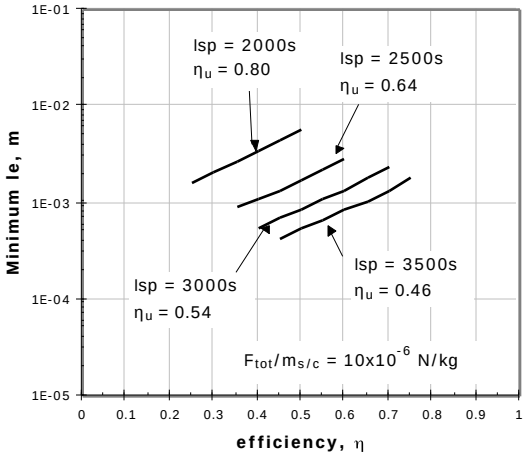


Figure 24. Minimum $l_e$ for $F_{tot}/m_{s/c} = 10 \times 10^{-6}$ N/kg

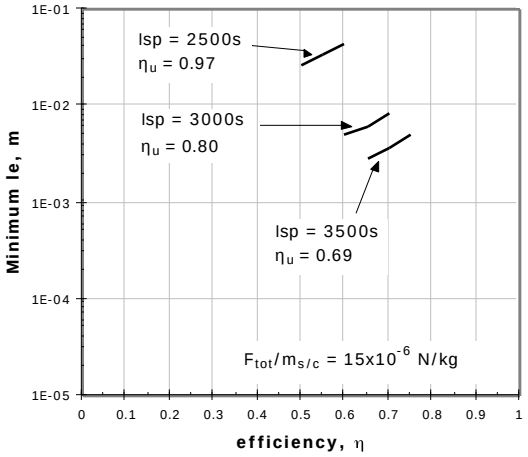


Figure 25. Minimum $l_e$ for $F_{tot}/m_{s/c} = 15 \times 10^{-6}$ N/kg

4.4 Preliminary Designs

The values of $V_{tot}$, $d_a$, and $\eta_u$ which led to minimization of $l_e$ at each combination of Isp and $\eta$ can now be used to generate preliminary designs of the linear ion microthruster.

The quantity $V_{tot}^{3/2} / d_a^2$ specifies $A_c N_c$ by equation (24). To produced an approximately square thruster,

$$L_c = \sqrt{2 A_c N_c}$$

where the factor of 2 assumes the walls separating the chambers have the same width as the chambers.

The width of the chamber can be found from

$$Wc = \frac{(A_c N_c)}{L_c N_c}$$

where $N_c$ is chosen to produce a reasonable value of $W_c$. Finally, with $N_c$ chosen, the quantity $A_c N_c$ and be solved for $A_c$.

The height of the chamber can be, to first order, chosen arbitrarily without altering the minimum $l_e$. This is due to the fact that the neutral density in the chamber (equation 22) is a function only of the chamber exit area if $\dot{m}$ is constant. More intuitively, increasing $H_c$ initially decreases neutral density because the chamber volume increases. However, the rate at which neutrals are lost from the chamber also decreases by the same amount since[15]

$$\dot{n}_o = \frac{1}{4} n_o e v_n A_c \phi_o$$

Therefore, if $\dot{m}$ is constant, $n_o$ and $\dot{n}_o$ and will increase back to their original levels. If the neutral density is not affected by a change in chamber height, then the probability that the primary electron will have a collision, $1-\exp[-\sigma_o n_o l_e]$, also remains unchanged.[15] The bottom line is that the primary electrons are just as effective as ionizers and no additional energy per beam ion needs to be expended.

A linear ion microthruster producing 1.5 mN of thrust on-board a 100 kg satellite (15μN per kg of spacecraft) could, from Figure 25, operate at $I_{sp}$=3000s, $\eta$=.65, $\eta_u$=0.80. Total voltage across the acceleration region is 736 V although there is no actual grid through which the ions accelerate. The minimum allowable primary electron confinement length is approximately, $l_e$ = 6 mm. To produce square thruster, chamber length, $L_c$, equals 2 mm. Choosing a 10 chamber configuration results in a chamber width of 0.1 mm. The chamber height, $H_c$, is chosen to equal 1 mm. Therefore, the normalized primary electron confinement length, $l_e/H_c$= 6. These preliminary dimensions are shown in Figure 26.

## 5. Future Work

Continuation of this work will focus on analysis of linear ion microthruster designs. A code developed by Arakawa[17] which predicts the performance of cusped ion thrusters will be modified for the scale, geometry and confinement mechanism of the linear ion microthruster. The code implements the Brophy model using a value of primary electron confinement length determined by a Monte Carlo simulation of primary electron motion within the discharge chamber. Based on experience gained in implementing the Arakawa code, the Particle-in-Cell (PIC) code developed at MIT to predict the solar array arcing phenomenon, will also be adapted to the microthruster's geometry and scale. Modification of the PIC code for the linear ion microthruster will allow prediction of energy cost per beam ion, the propellant utilization factor, and the fraction of ions extracted into the beam.

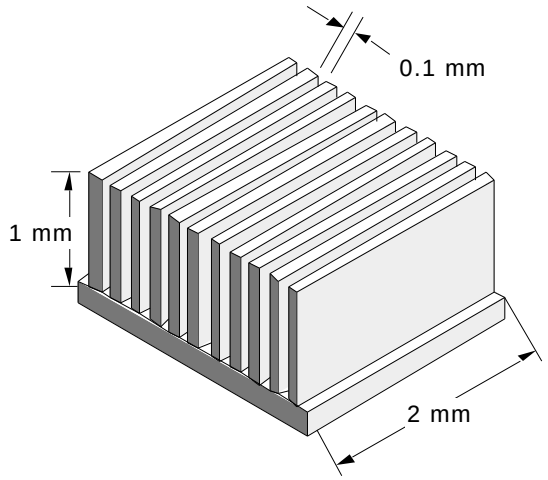


Figure 26. Preliminary sizing of Linear Ion Microthrusters

## 6. Summary and Conclusions

This paper has examined the propulsion system requirements for maintaining a local satellite cluster formation in Earth's orbit for the purpose of forming sparse aperture arrays. Near continuous thrusting by the propulsive system was found necessary to maintain the relative positions of the satellites within allowable tolerances. Satellite mass, volume, and power constraints limit reasonable cluster baselines to approximately 30 m, 300 m, and 5000 m at 1000 km, 10,000 km, and GEO altitudes respectively. To maintain these cluster baselines, the propulsive system must operate at minimum $I_{sp}$ and efficiency equal to approximately 3000s and 65% respectively with a thrust/spacecraft mass ratio of approximately 15μN/kg. A linear ion microthruster of this type could have dimensions 2mm x 2mm x 1mm, with 10 discharge chambers each 0.1 mm wide. The resulting primary electron confinement length would then be 6 times the chamber height.

## References


1. Swift, C. T. "Terrestrial Sensing with Synthetic Aperture Radiometers." IEEE MTT-S International Microwave Symposium Digest, vol. 1, p. 387-388, Boston MA, June 10-14, 1991.

2. Larson, W. J., Wertz, J. R. (editors), Space Mission Design and Analysis 2nd ed. pp. Kluwer Academic Publishers, Boston, 1992.

3. Wall, J.V., Modern Technology and Its Influence on Astronomy. Cambridge University Press, Cambridge, 1990.

4. Stachnik, R., Labeyrie, A. "Astronomy from Satellite Clusters." Sky and Telescope, pp 205-209, March 1984.

5. Heimiller, R.C., Belyea, J.E., Tomlinson, P.G., "Distributed Array Radar." IEEE Transactions on Aerospace and Electronic Systems vol. AES-19, No. 6, November 1983.

6. F. P. Schloerb, "Imaging Interferometry: Lesson from the Ground." SPIE Proceedings vol. 1947, pp 249-260, Orlando, FL. April 15-16, 1993.

7 R. Wohlleben, H. Mattes, T.H. Krichbaum, Interferometry in Radioastronomy and Radar Techniques. Kluwer Academic Publishers, Boston, 1991.

8. Prussing, J.E., Conway, B.A. Orbital Mechanics, Oxford University Press, New York, 1993.

9. S.W. Janson, "The On-Orbit Role of Electric Propulsion." AIAA 93-2220, 29th Joint Propulsion Conference and Exhibit, June 28-30, 1993, Monterey, CA.

10. Sutton, G.P., Rocket Propulsion Elements 6th ed., John Wiley & Sons, Inc., New York, 1992.

11. G. Malyshev et. al. "Comparative Analysis of the Propulsion System for the Small Satellite", IEPC-95-156, 24th International Electric Propulsion Conference, Moscow, Russia, Sept. 19-23, 1995.

12. Brophy, J.R. et al. "Ion Thruster-On-A Chip for Microspacecraft" unpublished white paper. Jet Propulsion Lab. April 26, 1995.

13. Cho, M.. "Arcing in High Voltage Solar Arrays in Low Earth Orbit: Theory and Computer Particle Simulation", Ph.D. Thesis, MIT, 1992.

14. Perez de la Cruz, C. "Arc Rate Predictions and Flight Data Analysis, for the Solar Array Module Plasma Interactions Experiment (SAMPIE)", S.M Thesis, MIT, 1995.

15. Brophy, J.R., Wilbur, P.J., "Simple Perfromance Model for Ring and Line Cusp Ion Thrusters" AIAA Journal pp. 1731-1736, 23 No. 11, November 1985.

16. Martinez-Sanchez, M., Course Handout: 16.522 Space Propulsion, Fall 1995, MIT.

17. Arakawa, Y., Ishihara, K., "A Numerical Code for Cusped Ion Thrusters." IEPC-91-118, 22nd International Electric Propulsion Conference, Oct. 14-17, 1991, Viareggio, Italy.